Journal of South American Earth Sciences 92 (2019) 145–150

Contents lists available at ScienceDirect

Journal of South American Earth Sciences

journal homepage: www.elsevier.com/locate/jsames

Remotely sensed survey of landslide clusters: Case study of Itaoca, Brazil

José A.N. Batista[a,*], Pierre Y. Julien[b]

[a] Water Resources Department, State University of Campinas, 224 Saturnino de Brito, Campinas, SP, Brazil
[b] Civil and Environmental Engineering Department, Colorado State University, 1320 Engineering Research Center, Fort Collins, CO, USA

ARTICLE INFO

Keywords:
Landslide clusters
Debris flow
Remote sensing

ABSTRACT

In January 2014, severe rainfall triggered landslides that buried 92 buildings and claimed 27 lives in the City of Itaoca (3000 inhabitants) in Brazil. The investigation of remotely sensed imagery and a ground-based weather radar shows a landslide cluster with 365 landslide scars over a quite uniformly vegetated background. The devastated area covers 33 km^2 with hillslopes ranging from 300 m to 1200 m in elevation, where intense rainfall reached 50 mm–170 mm within 2–6 h. The landslide slopes (median value at 26°) are in general steeper for low rainfall intensities and longer rainstorm durations. Landslide clusters behave in response both to rainfall spatial distribution and land slopes. The total scar area of landslide clusters of given median slope exhibits a peak curve with maximum at the overall median slope. The individual scar areas exceedance probability follows a log-gamma distribution and the scar surface area increases with slide slopes.

1. Introduction

Landslides are triggered by intense rainstorms which directly impact living populations and infrastructure. The acceleration of damages caused by landslides is becoming an increasing concern worldwide (Petley, 2012; Schuster, 1996). To define the rainfall threshold for landslides, Aleotti (2004) suggested that hyetographs cannot fully describe landslides because rain gauges cannot describe the spatial distribution of rainstorms. Melillo et al. (2015) point out the lack of criteria to precisely reconstruct landslide triggering hyetographs. Abancó et al. (2016) instrumented a field area to capture three torrential flow events consisting of 25 landslide triggers. Accordingly, 35% of the events happened before the peak rainfall intensity. Segoni et al. (2014) showed that the performance of a rainfall threshold is enhanced by considering soil slopes as a determining factor.

Landslide inventories are surveyed more accurately at a local scale where either stereoscopic images or accurate field topographic instruments are used for slope determination. In New Zealand, landslide inventories (De Rose, 2013) point to median slide slopes at 30°, while the median hill slope was 25° with a slide slope threshold at 20°. In general, the stability angle depends on the rainfall pattern, the surface slope angle and the geotechnical properties of the soil (Lu and Godt, 2013). Remotely-sensed terrain elevation data are available worldwide so that GIS can be used to determine terrain gradients (e.g. De Rose, 2013). Satellite borne terrain elevation radars frequently provide 30–90-m resolution data for landslide regional scale studies (Nichol et al., 2006; e.g. van Westen et al., 2006; Ahmed and Rogers, 2014). In areas covered by weather radars, hourly (or sometimes finer time intervals) rainfall data can be determined at a 2 km-grid, as used by von Ruette et al. (2014) for numerical experiments where the bedrock interface with the soil column is assumed as its failure plane. They examined the spatial variability of rainfall in relation to the number of landslides and volume of sediment, but warn their results are due to the model assumptions and parameter settings for the soil column failure. Such heterogeneous nature of rainfall spatial distribution and soil slopes strongly determine landslide statistics, and the lack of sufficiently available field data for deterministic dynamic-flow simulations has motivated research on empirical methods (Iverson, 2014).

This study examines the spatial-frequency of both slide slope and scar areas from the landslide scars observed in the City of Itaoca in southeastern Brazil. Such variables have been pointed by Malamud et al. (2004) and De Rose (2013) as key factors towards landslide hazard assessment in terms of soil waste release volume. In total, 365 shallow landslides are examined within a squared region of 33 km^2. The distribution of slide slopes and scar areas are examined with respect to precipitation obtained from a ground weather radar in clusters to each radar grid cell and to topographic information from a Geographic Information System (GIS).

2. Study area

The Brazilian Atlantic Highlands landform extend alongside the Atlantic Ocean from latitude 15 to 30°S where the highest population

* Corresponding author.
E-mail address: nbatista@fec.unicamp.br (J.A.N. Batista).

https://doi.org/10.1016/j.jsames.2019.02.021
Received 5 March 2018; Received in revised form 27 February 2019; Accepted 27 February 2019
Available online 15 March 2019
0895-9811/

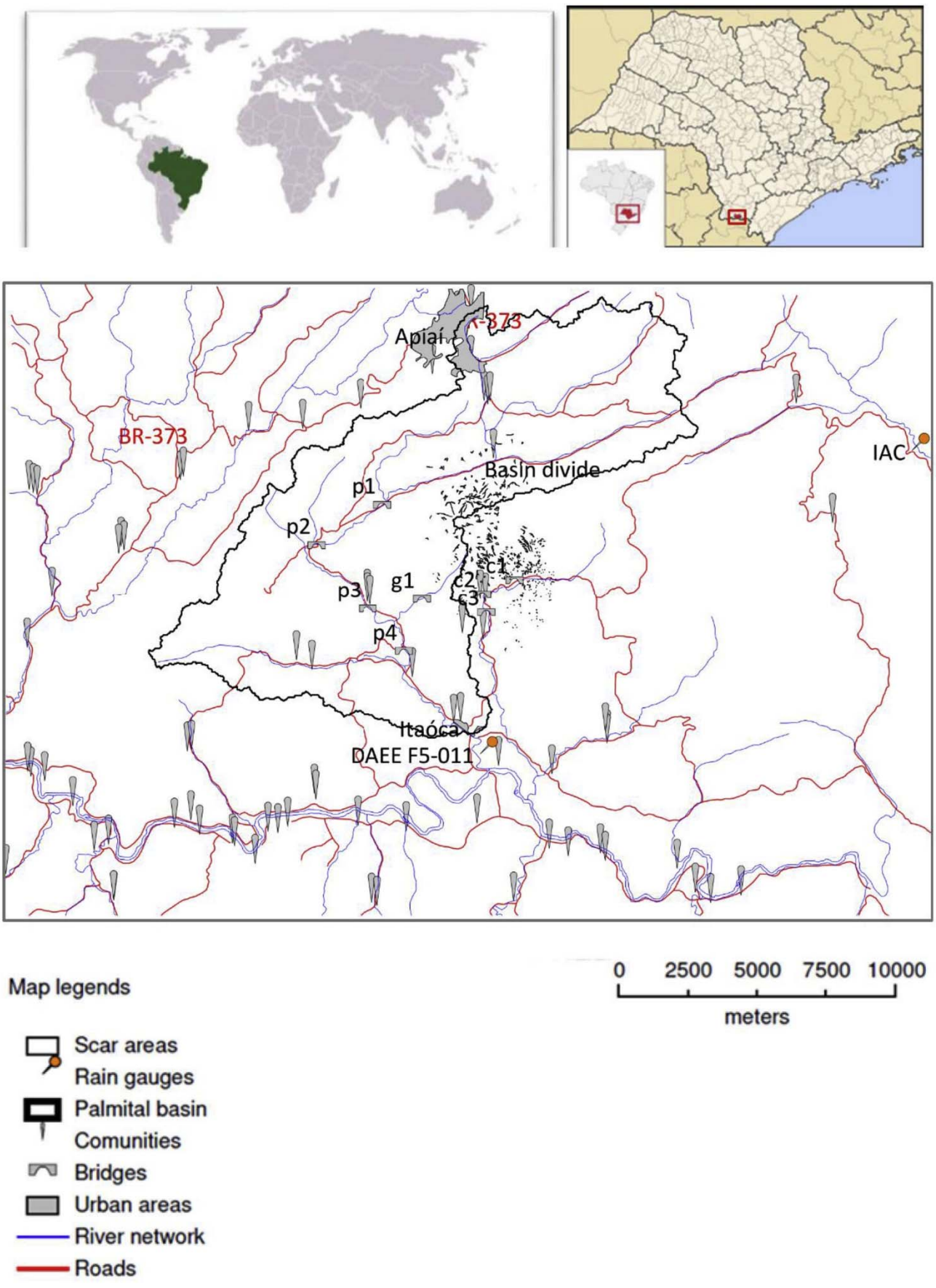

Fig. 1. Study area around Itaoca. The city of Itaoca is at coordinates 48°50′19″W and 24°38′29″S.

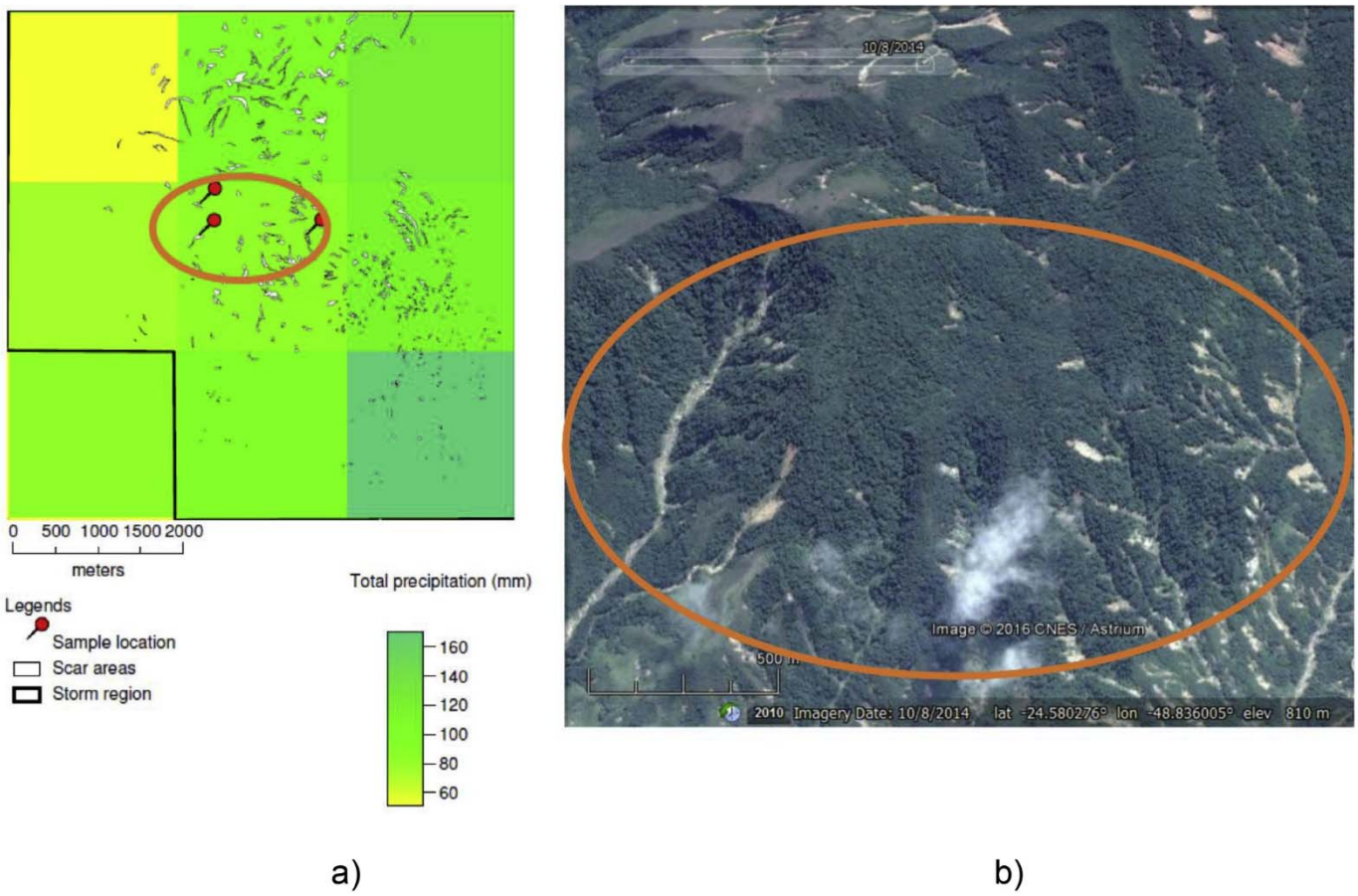

Fig. 2. Precipitation totals as estimated from radar data over the study area (the ellipse indicates the middle third of landslides). a) Spatial distribution of shallow landslide scars, as well as sampling locations. b) Satellite clipped image for scars in a radar grid cell. The center of the image clip is at coordinates 24°34′49″S and 48°50′10″W.

density is located. This landform consists in general of 12-m deep acrisols and ferralsols (Hengl et al., 2014) originally covered by the Atlantic Forest. The annual rainfall rate spans from 1000 mm to 2000 mm. The City of Itaoca (3000 inhabitants) was founded in 1991 at the coordinates 48°50′19″W and 24°38′29″S at an elevation of 143 m (Fig. 1). In January 2014, a heavy rainfall triggered 365 shallow landslides burying 92 buildings and causing 27 fatalities. Six bridges collapsed: (1) two along 7-km of the Palmital River (points p1 and p3 on Fig. 1); (2) one over its tributary Guarda-mao (g1); and (3) three others outside the Palmital basin on Curutuva Creek (c1, c2 and c3). Daily precipitation records in Fig. 1 from rain gauge station DAEE F5-011 point to an annual rainfall averaging 1375 mm. The overland elevation ranges from 133 to 1200 m in altitude in this 700 km^2 study area.

In Itaoca, the landslides happened mostly alongside 8 km of the Palmital basin divide, which bounds 134 km^2. The scars were surveyed by searching the August-10th 2014 GeoEye® multi-spectral optical images (1.65-m resolution) and verified with the January 21st, 2014 panchromatic images (0.41-m resolution) provided by CSNE/Astrium© and Google©. Surveying scar areas in Itaoca has been possible through the uniform vegetation background by using the satellite multi-spectral image released nine months after the storm. Terrain elevation data and morphologic parameters are estimated with the SRTM (Farr et al., 2007) 1 arc-sec resolution (30 × 30 m^2) radar imagery (USGS, 2006). This visual interpretation allowed the identification and segmentation of 365 landslide scars.

Geologic formations include calc-alkaline granite, metasandstone, metasiltstone and marble, which have been weathered to non-cohesive and non-plastic soils (Chieregati, 2008). These weathered rock formations contain low proportions of silt and clay, and a majority of fine and coarse sand. Hungr et al. (2014) revisited the Varnes classification of landslides to define debris as the mixture of non-plastic to low-plastic sand, gravel, cobbles and boulders often with varying portions of silt and clay. Hungr et al. (2014)use the term debris slides to represent homogeneous non-cohesive granular solids on hillslopes 20°–30° steep. Multiple landslides in these materials may release tens of thousands of cubic meters of sediment as debris avalanches triggered by heavy rainfalls. As recorded in the optical images, most of the debris avalanche scars are comparably small and shallow, typically provoked by the heavy rainfall there was in this event. Debris flows were also observed alongside the Guarda-Mao stream (shown in Fig. 1 by the g1 bridge) where the first order stream showed cobbles and boulders. The deposition area of these landslide runouts is located downstream of the Palmital river.

3. Rainfall precipitation

The rain gauge network in the study area includes two stations at: (1) IAC-Itaoca (48°41′1.7″W and 24°32′58.2″S, 185-m elevation); and (2) DAEE F5-011 (48°49′59.9″W and 24°38′59.9″S, 180-m elevation). The station IAC-Itaoca is part of the CIIAGRO weather monitoring network since 2011 (Abramides et al., 2015). The rain gauge station DAEE F5-011 is part of the DAEE rainfall monitoring network (Borsari and Araujo, 2010), whose data series spans from 1963 to 2000, and a maximum daily precipitation of 137.5 mm was measured in 1995. The rain gauge IAC-Itaoca was damaged during the storm of this study and no precipitation direct measurement is available. Rainfall duration and intensity could only be estimated from remote sensing equipment. Weather radars provide data at a high space-time resolution (i.e. 10 min

data and 2 by 2 km grid cells). MAXCAPPI radar images are available for the study area from the Sao Roque radar station (23°36′07″S, 47°5′39″W, 1147-m elevation), which is part of the Brazilian Air Force radar network, also called REDEMET (Henriques et al., 2010). Such images are formed at three elevation angles (0.5°, 1.5° and 2.5°). Since the radar covers 400 km maximum in radius, the Itaoca landslide area is located as far as 212 km from the radar; the vertical radar coverage at that place ranges from 4 to 13-km in elevation. Rainfall intensities (R in mm/h) are estimated from the radar reflectivity (Z in dBZ) after using the theoretical (Joss et al., 1970; Marshall and Palmer, 1948) or the empirical Z-R relationships (Rosenfeld et al., 1993). According to Rosenfeld et al. (1993) the theoretical rain drop distribution systematically underestimate tropical storms, leading them to propose an accurate empirical formula for a Z-R relationship in the Southeastern Hemisphere (12°15′0″S, 130°33′36″E) as:

$$Z = 230R^{1.25} \quad (1)$$

The Rosenfeld et al. (1993) relationship is applied to this study. Radar imagery of 2014-01-12 20:40 through 2014-01-13 04:10 UTC showed precipitation span in the landslide area from 51 to 170 mm, accumulated in 6.5 h (Fig. 2a). Such results are comparable with the historical rain gauge data span formerly registered in the Palmital river valley in downtown Itaoca.

Rainfall intensities and durations are surveyed in the Itaoca landslide area by the storm event ranged from 7.4 to 55.4 mm/h and durations ranged from 2.2 to 6.5 h over the scars. Fig. 3a shows the frequency distribution of rainfall depth over the landslide area, with eight readings from the $2 \times 2\,km^2$ radar data, in comparison to the regional precipitations. The rainfall records at Itaoca showed no antecedent precipitation during the period of five days prior to the landslides (Abramides et al., 2015). Shallow landslides are triggered by storms with a short duration and high intensity. Intense rain storms rapidly add weight to the soil subsurface and reduce the suction head of the soils during the infiltration process (Lu and Godt, 2013).

4. Slide slope threshold and scars

Three landslide scars have been sampled using a standard penetration test (SPT) to represent the landslide scars for soil texture, considering those landslide scars close to the scatter middle third, as indicated in Fig. 2. The soil texture classification confirms that the soil is non-cohesive, being found as a sandy clay, as typically present in residual soils of calcareous rock. Table 1 summarizes soil sampling data that represents soil texture at landslide scars, and the Itaoca soils have no (or a low) cohesion. Gramani and Martins (2016) present a detailed photographic survey, which shows riverbank vegetation profile and debris deposited downhill throughout streams. The downhill vegetation is typically a dense evergreen rain forest and pastures. Uphill, the watershed soil is occupied by a dense evergreen rain forest. Although vegetation can play an important role contributing to soil stability, root cohesion has not been considered in this study.

Regarding the survey of the distribution of slide slope, the elevation data and optical images have been overlaid. Scars have been visually delineated from the detailed terrain data and aforementioned satellite images. Surface areas have been calculated as irregular polygons. The scar's centroid coordinates were taken from the land cover images and slope angles inside the scars were obtained from the elevation raster map in GRASS GIS (distributed under the General Public License from GNU organization, GPL/GNU). The regional terrain slope follows a gamma distribution with a median slope of 17° (Fig. 3b). In contrast, the median slope for the landslides is 26°. The extreme slide slopes were observed where soils are unconditionally unstable (about 50°). For sake of a comparison basis, in the 2011 Nova Friburgo's 3562 landslides ($32{,}000\,km^2$) in southeastern Brazil (Avelar et al., 2013), the median slide slope of 20° was found also steeper than the overland slope median of 17° (same terrain slope as Itaoca). The slide slope threshold in Nova Friburgo could not be determined, but Avelar et al. (2013) defined the lowest quartile of the slide slopes at 11°. Fig. 3b shows, in general, that the Nova Friburgo slide-slope angles are lower than Itaoca's. The precipitation event that triggered landslides totaled 135 mm of rain in 8 h while in Nova Friburgo the precipitation reached 325 mm in 48 h. The unconditionally unstable slope, where the basement rock outcrops is evidenced in Fig. 3c, reached 60° at Nova Friburgo, while only 50° for Itaoca.

Fig. 3c plots rainfall intensities grouped by rainfall durations and landslide slopes. The landslide slopes are generally steeper for low rainfall intensities and longer rainstorm durations. The slide slopes' locations are queried in GIS as a function of rainfall intensity and duration. It is also seen from that landslide slope span that a slope threshold should exist around 10° as shown in Fig. 3c. Slide slopes lower than 10° are also present, mostly under high rainfall intensities (55.4 and 36.0 mm/h). Such slide slope thresholds for each rainfall intensity are empirically determined to the confidence level of 90% as presented in Table 2. The unconditionally unstable hillslope angle is obtained in Fig. 3c and no landslide lies steeper than 55°. This is consistent with the results shown in Fig. 3b. Based on such behavior of slide slopes against rainfall intensities, a timeline direction can be established starting on the steepest slopes and highest rainfall intensities in the direction of more stable slopes and lower rainfall intensities. This behavior has been noticed by studies about early warning (e.g. Aleotti, 2004) and rainfall triggering reconstitution (Abancó et al., 2016; Melillo et al., 2015) reinforce the idea that rainfall initiation shows a sharp increase in intensity.

The distribution of landslide areas in Itaoca is shown in Fig. 3d. The Itaoca's scars areas vary by five orders of magnitude, with a median of $493\,m^2$. Likewise, according to Avelar et al. (2013) the landslide scar areas in Nova Friburgo also vary by similar orders of magnitude, with a much higher median equal to $1{,}085\,m^2$. This wide range of values leads the scar areas frequency distribution to be gamma distributed over several log cycles (log-gamma). The sediment volume is also dependent both on the slide slope-frequency (De Rose, 2013; Malamud et al., 2004) and on the spatial distribution of rainfall (von Ruette et al., 2014). Scar areas and scar volumes are related by the area-volume relationship curve (Malamud et al., 2004). De Rose (2013) analyzed the effect of slopes on the sediment release as a cause for the density of landslides (the land coverage by scars). This behavior is well observed in Fig. 4a after plotting the total scar area against median slide slopes as taken in each radar grid cell. The total scar area decreases in value as much as the slide slope deviate from the overall median slide slope (26°). The total scar area throughout such clusters spans over two orders of magnitude, from 5000 to $203{,}000\,m^2$. Such shorter variability leads to a non-logarithmic frequency distribution type gamma. The scar areas have been ploted herein according to slide slopes, as clustered by each radar grid cell. As a result, the total scar area distribution with slide slope plots like a peak curve shown in Fig. 4a.

Table 2 summarizes the precipitation depths obtained for each scar group by radar grid cells (including rainfall intensity and duration), the landslide slope thresholds (90% confidence level), the median landslide slope, the number of scars and the total landslide scar area. Precipitations in Table 2 relates to radar grid cells of Fig. 2a with the first three rows corresponding to the top three radar grid cells from left to right, and so on.

Fig. 4b shows how scar area increases with slide slope. Landslides starting on steep slopes typically route material downstream as debris flow. The flow momentum increases the scar length and area as the debris material propagates downstream (Hungr et al., 2014). The distribution of scar areas obtained herein does exhibit the debris flow routing effect over scars on steeper slide slopes. Therefore, the scar individual areas increasing to each slide slope shown in Fig. 4b is indeed resulting from landslide scars as affected by debris flow routing downstream. In comparison, landslides observed by De Rose (2013) did not start soil runouts (e.g. debris flow), so those landslides are not

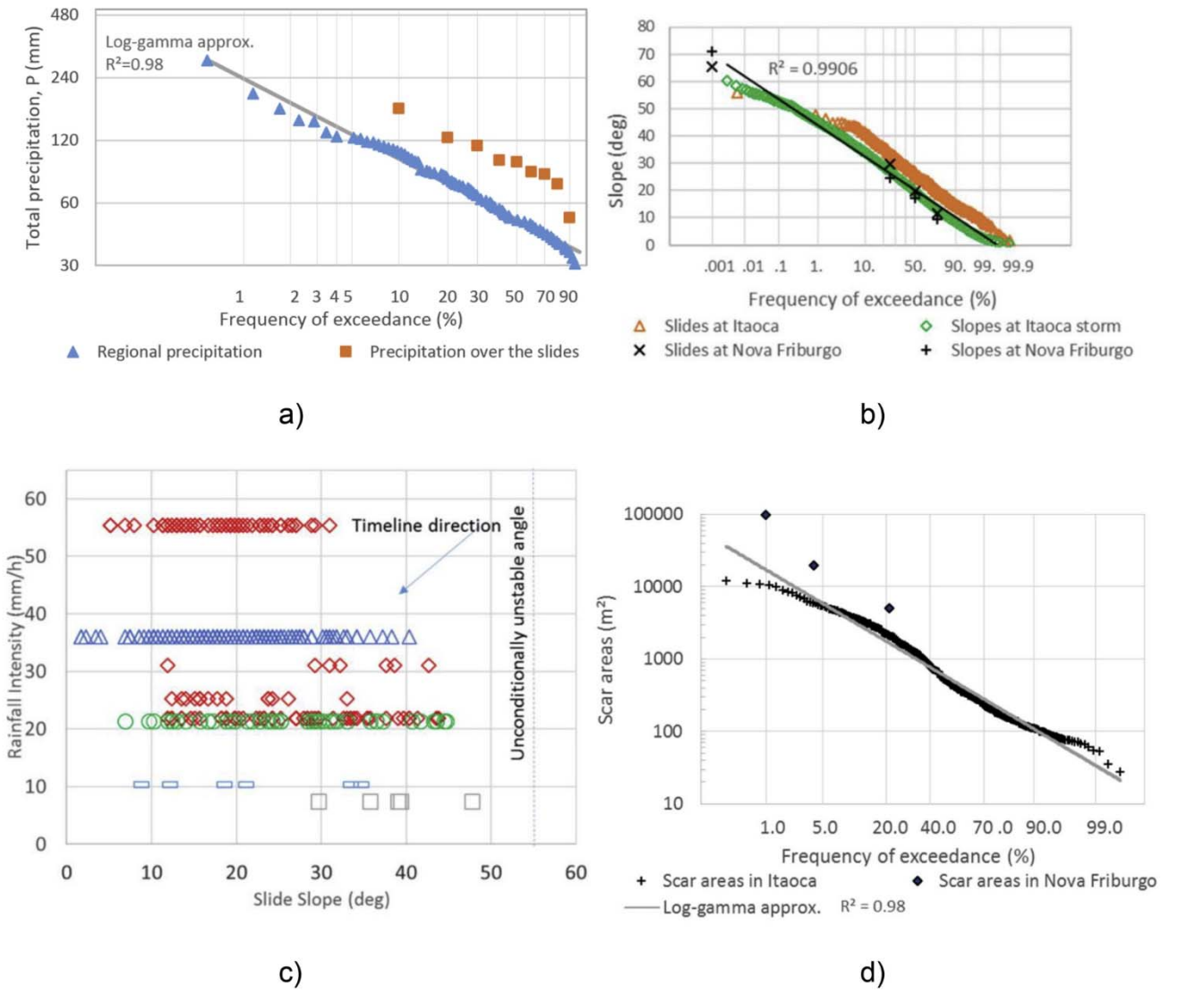

Fig. 3. Spatial distributions and landslide threshold in Itaoca and Nova Friburgo. a) Rainfall depth for the landslide area and the storm region. b) Slide slope gamma frequency over the terrain slope. c) Landslide threshold for rainfall intensity and duration. d) Scar area distribution.

Table 1
Soil sampling dataset.

Sample	Real density (−)	Porosity (%)	Soil texture
1	2,15	17,00	sandy clay
2	2,11	16,00	sandy clay
3	2,12	14,00	sandy clay

routed downstream, and scars even in steeper slopes show no accretion. Hence, the distribution of scar areas with slide slopes (Fig. 4b) apparently diverges from the results of De Rose (2013).

5. Conclusion

With the aid of satellite born landcover pancromatic images, observations were made possible for a landslide cluster over a quite uniformly vegetated background. It was then possible to use SRTM terrain elevation data and rainfall measurements from weather radar to correlate rainfall precipitation with slide slope and scar area for 365 landslide scars at Itaoca in Brazil. The method of surveying such data is divided in two steps: i) querying minimal slopes related to spatialized rainfall intensity data; and ii) querying scar areas individually related to

Table 2
Summary of precipitation, landslide slopes and scar areas by radar grid cell in Itaoca.

Precipitation (mm)	Intensity (mm/h)	Duration (hours)	Minimumslide slope (°)	Median slide slope (°)	Number of scars	Total scar area (ha)
45.5	7.4	6.50	19.0	39.0	5	1.76
52.5	21.3	2.50	14.0	25.2	53	20.34
67.3	31.0	2.17	12.7	32.2	7	1.84
55.0	10.3	5.50	15.5	19.0	6	0.60
45.6	21.8	2.17	14.8	26.1	62	16.44
81.6	36.0	2.33	13.1	20.3	162	10.70
54.3	25.2	2.17	13.9	16.7	15	0.46
119.4	55.4	2.17	11.5	18.8	55	1.53

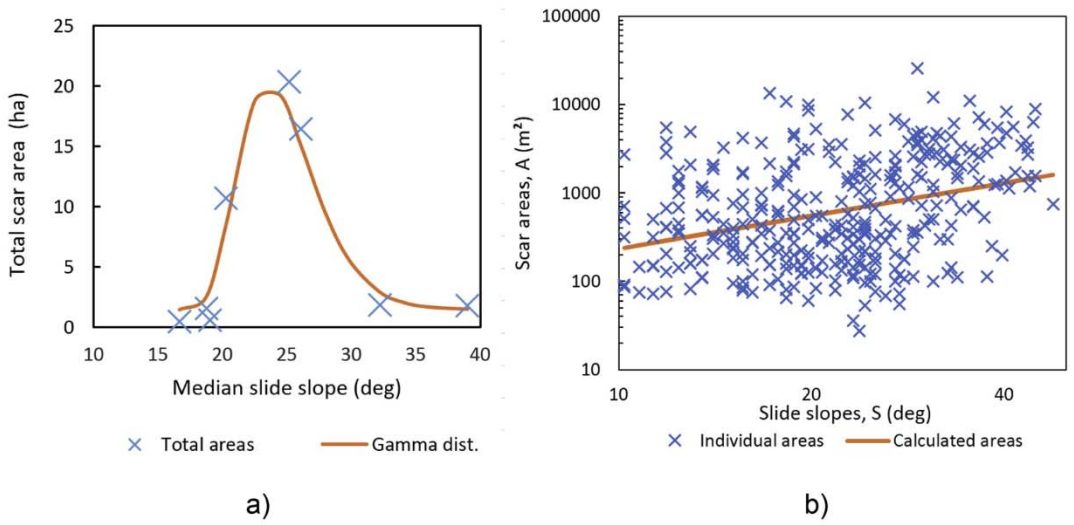

Fig. 4. Distribution of landslide scar areas versus slide slope: a) total number in each radar grid cell, b) individual values.

each slide slope. As a result, the scar areas have showed, on one hand, a consistently increasing trend with the slide slope failure angle. On the other hand, the total scar area of landslide clusters exhibits a peak curve with maximum at the overall median slope. The largest scars are found on the steeper slopes and the frequency of scar areas follows a log-gamma distribution. The spatial distribution of rainfall depths has been observed to be higher over the landslide devastated area. The slide slopes showed steeper than the land slopes for each exceedance frequency. The results obtained herein also indicate that there is a slope failure angle threshold sensitive to rainfall intensity and duration, such that rainstorms with lower intensities and longer durations trigger landslides on steeper slopes, and vice-versa.

Acknowledgements

The authors thank the São Paulo Research Foundation for granting a post-doctoral scholarship to Jose Batista (2014/12237-8) in support of his research at Colorado State University.

References

Abancó, C., Hürlimann, M., Moya, J., Berenguer, M., 2016. Critical rainfall conditions for the initiation of torrential flows. Results from the Rebaixader catchment (Central Pyrenees). J. Hydrol. https://doi.org/10.1016/j.jhydrol.2016.01.019.

Abramides, P., Brunini, O., Pedro Júnior, M., Camargo, M., Ernandes, E., Blani, G., Brunini, A., Brigante, R., Santos, R., 2015. Web Portal Integrated Center for Agrometeorologic Information. Campinas.

Ahmed, M.F., Rogers, J.D., 2014. First-approximation landslide inventory maps for Northern Pakistan, using ASTER DEM data and geomorphic indicators. Environ. Eng. Geosci. 20, 67–83. https://doi.org/10.2113/gseegeosci.20.1.67.

Aleotti, P., 2004. A warning system for rainfall-induced shallow failures. Eng. Geol. 73, 247–265. https://doi.org/10.1016/j.enggeo.2004.01.007.

Avelar, A., Netto, A.C., Lacerda, W., Becker, L., Mendonça, M., 2013. Mechanisms of the recent catastrophic landslides in the Mountainous range of Rio de Janeiro, Brazil. In: Margottini, C., Canuti, P., Sassa, K. (Eds.), Landslide Science and Practice SE - 34. Springer Berlin Heidelberg, pp. 265–270. https://doi.org/10.1007/978-3-642-31337-0_34.

Borsari, R.D., Araujo, L.M., 2010. Web Portal for Hydrologic Information of Uphill Tiete River Basin. (Sao Paulo).

Chieregati, L.A., 2008. Geological Map Plant Apiaí. 1:100.000. SG.22-X-B-V.

De Rose, R.C., 2013. Slope control on the frequency distribution of shallow landslides and associated soil properties, North Island, New Zealand. Earth Surf. Process. Landforms 38, 356–371. https://doi.org/10.1002/esp.3283.

Farr, T.G., Rosen, P.A., Caro, E., Crippen, R., Duren, R., Hensley, S., Kobrick, M., Paller, M., Rodriguez, E., Roth, L., Seal, D., Shaffer, S., Shimada, J., Umland, J., Werner, M., Oskin, M., Burbank, D., Alsdorf, D., 2007. The shuttle radar topography mission. Rev. Geophys. 45, RG2004. https://doi.org/10.1029/2005RG000183.

Gramani, M., Martins, V., 2016. Debris flows occurrence by intense rains at Itaoca city, São Paulo, Brazil: field observations. In: Aversa, Stefano, Cascini, Leonardo, Luciano Picarelli, C.S. (Eds.), Landslides and Engineered Slopes. Experience, Theory and Practice Proceedings of the 12th International Symposium on Landslides. Taylor & Francis Group, Napoli (Chapter 110).

Hengl, T., de Jesus, J.M., MacMillan, R.A., Batjes, N.H., Heuvelink, G.B.M., Ribeiro, E., Samuel-Rosa, A., Kempen, B., Leenaars, J.G.B., Walsh, M.G., Gonzalez, M.R., 2014. SoilGrids1km — global soil information based on automated mapping. PLoS One 9, 1–17. https://doi.org/10.1371/journal.pone.0105992.

Henriques, C., Tessarolli, G., Castro, J., 2010. Application Programming Interface REDEMET. (Rio de Janeiro).

Hungr, O., Leroueil, S., Picarelli, L., 2014. The Varnes classification of landslide types, an update. Landslides 11, 167–194. https://doi.org/10.1007/s10346-013-0436-y.

Iverson, R.M., 2014. Debris flows: behaviour and hazard assessment. Geol. Today 30, 15–20. https://doi.org/10.1111/gto.12037.

Joss, J., Schram, K., Thams, J.C., Waldvogel, A., 1970. On the Quantitative Determination of Precipitation by Radar. Svizzera, Locarno-Monti, Switzerland.

Lu, N., Godt, J.W., 2013. Hillslope Hydrology and Stability. Cambridge University Press.

Malamud, B.D., Turcotte, D.L., Guzzetti, F., Reichenbach, P., 2004. Landslide inventories and their statistical properties. Earth Surf. Process. Landforms 29, 687–711. https://doi.org/10.1002/esp.1064.

Marshall, J.S., Palmer, W.M.K., 1948. The distribution of raindrops with size. J. Meteorol. 5, 165–166. https://doi.org/10.1175/1520-0469(1948)005<0165:TDORWS>2.0.CO;2.

Melillo, M., Brunetti, M.T., Peruccacci, S., Gariano, S.L., Guzzetti, F., 2015. An algorithm for the objective reconstruction of rainfall events responsible for landslides. Landslides 12, 311–320. https://doi.org/10.1007/s10346-014-0471-3.

Nichol, J.E., Shaker, A., Wong, M.-S., 2006. Application of high-resolution stereo satellite images to detailed landslide hazard assessment. Geomorphology 76, 68–75. https://doi.org/10.1016/j.geomorph.2005.10.001.

Petley, D., 2012. Global patterns of loss of life from landslides. Geology 40, 927–930. https://doi.org/10.1130/G33217.1.

Rosenfeld, D., Wolff, D.B., Atlas, D., 1993. General probability-matched relations between radar reflectivity and rain rate. J. Appl. Meteorol. 32, 50–72. https://doi.org/10.1175/1520-0450(1993)032<0050:GPMRBR>2.0.CO;2.

Schuster, R.L., 1996. The 25 most catastrophic landslides of the 20th century. In: Chacon, J., Irigaray, C., Fernandez, T. (Eds.), Proc. Of the 8th International Conf. & Field Trip on Landslides. Balkema, Granada.

Segoni, S., Rosi, A., Rossi, G., Catani, F., Casagli, N., 2014. Analysing the relationship between rainfalls and landslides to define a mosaic of triggering thresholds for regional-scale warning systems. Nat. Hazards Earth Syst. Sci. 14, 2637–2648. https://doi.org/10.5194/nhess-14-2637-2014.

USGS, 2006. Shuttle Radar Topography Mission. Arc Second Scenes. Filled Finished 2.0.

van Westen, C.J., van Asch, T.W.J., Soeters, R., 2006. Landslide hazard and risk zonation—why is it still so difficult? Bull. Eng. Geol. Environ. 65, 167–184. https://doi.org/10.1007/s10064-005-0023-0.

von Ruette, J., Lehmann, P., Or, D., 2014. Effects of rainfall spatial variability and intermittency on shallow landslide triggering patterns at a catchment scale. Water Resour. Res. 50, 7780–7799. https://doi.org/10.1002/2013WR015122.